

Large output voltage to magnetic flux change in nanoSQUIDs based on direct-write Focused Ion Beam Induced Deposition technique

Fabian Sigloch^a, Soraya Sangiao^{a,b}, Pablo Orús^a, and José María de Teresa^{a,b,*}

^aInstituto de Nanociencia y Materiales de Aragón (INMA),
Universidad de Zaragoza-CSIC, 50009 Zaragoza, Spain

^bLaboratorio de Microscopías Avanzadas (LMA), Universidad de Zaragoza, 50018, Spain

*E-Mail: determina@unizar.es

March 11, 2022

Abstract

NanoSQUIDs are quantum sensors that excel in detecting a small change in magnetic flux with high sensitivity and high spatial resolution. Here, we employ resist-free direct-write Ga^+ Focused Ion Beam Induced Deposition (FIBID) techniques to grow W-C nanoSQUIDs, and we investigate their electrical response to changes in the magnetic flux. Remarkably, FIBID allows the fast (3 min) growth of $700 \text{ nm} \times 300 \text{ nm}$ Dayem-bridge nanoSQUIDs based on narrow nanowires (50 nm wide) that act as Josephson junctions. The observed transfer coefficient (output voltage to magnetic flux change) is very high (up to $1301 \mu\text{V}/\Phi_0$), which correlates with the high resistivity of W-C in the normal state. We discuss here the potential of this approach to reduce the active area of the nanoSQUIDs to gain spatial resolution as well as their integration on cantilevers for scanning-SQUID applications.

1 Introduction

Direct current- (dc-) Superconducting Quantum Interference Devices (SQUIDs) are magnetic flux sensors that attain an unrivaled sensitivity [1, 2] by exploiting the physical effects of magnetic flux quantization [3] and Josephson effect [4]. A dc-SQUID consists of a superconducting ring interrupted by two Josephson junctions (JJs), one on either side (fig. 1a). A JJ is formed by a superconductor (S) interrupted by either an insulator (I), a normal metal (N) or a weaker superconductor (s) resulting, respectively, in a SIS-, SNS- or SsS-junction that is capable of carrying a superconducting Josephson current, I_J . The flux quantization within the superconducting ring is attained by the induction of a loop current, J , which either opposes or supports the external magnetic field, lowering or rising the flux threading the ring to an integer multiple of the magnetic flux quantum,

Φ_0 . The bias current, I_b , injected into one of the arms of the SQUID splits into two phase-sensitive Josephson currents running simultaneously through both of the JJs and interfering in the second arm.

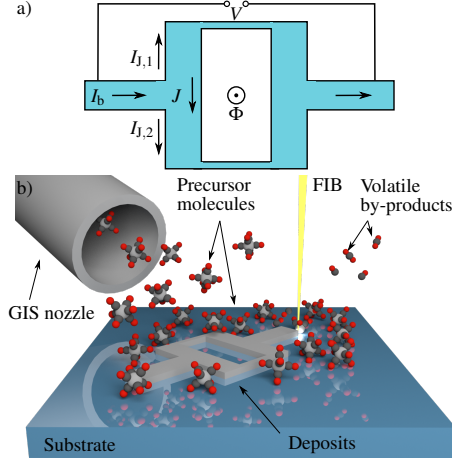


Figure 1: a) Schematic working principle of a dc-SQUID. A constant bias current I_b is injected. It splits up into two Josephson currents $I_{J,i}$ running through the Josephson junctions on either side of the SQUID. A loop current J is induced to lower or raise the flux Φ threading the SQUID loop to an integer multiple of the magnetic flux quantum Φ_0 . For $I_b \sim I_c$ a flux-dependent voltage V drops across the SQUID. b) Schematic working principle of Focused Ion Beam Induced Deposition (FIBID). The precursor molecules are locally decomposed by irradiation with the Focused Ion Beam (FIB). The metallic constituents remain on the substrate constituting the deposit, the volatile by-products are removed by the vacuum system of the instrument.

The sensitivity of SQUIDs is limited by the flux noise, S_Φ , and the SQUID inductance, L . The flux noise can be reduced by downsizing of the dimensions of the JJs [5], whereas the inductance can be reduced by decreasing the size of the effective inner SQUID area [6]. Ever since this revelation a lot of effort has been brought forth and various methods have been developed to fabricate *nanoSQUIDs* with ever lower geometrical dimensions and thus higher sensitivity [7, 8, 9].

While SQUIDs with SIS- or SNS-junctions commonly require a sandwich-type structure composed of multiple layers, SQUIDs based on SsS-junctions are planar and fabricated in a single layer. In this approach the JJs are realized by two constrictions in the SQUID loop, the Dayem Bridges (DBs) [10], forming regions with lower I_c in the superconducting material. The low thickness of the planar DB-nanoSQUIDs makes them insusceptible to in-plane fields and enables for good coupling to magnetic nanoparticles. However, the dissipation of heat in the normal-conducting state of the DBs yields a hysteretic I-V characteristic in materials with high I_c . Generally, the kinetic inductance, L_{kin} is high and can dominate the total inductance of the SQUID [1].

Conventionally, the design for a nanoSQUID is transferred to a resist by means of Electron Beam Lithography (EBL). The structure can either be deposited via evaporation of a superconducting material followed by lift-off or etched from a

previously patterned superconducting film [11]. Processes based on EBL are well established and allow for complicated geometries with linewidths down to 30 nm [5]. NanoSQUIDs based on DBs have been fabricated with an inner loop area of down to $200 \text{ nm} \times 100 \text{ nm}$ and a spin sensitivity of $\sim 10\,000 \mu_B/\sqrt{\text{Hz}}$ by means of EBL [11]. However, the resist-based EBL process requires multiple fabrication steps making it a time-consuming approach. A homogeneous film of the resist is obtained by spin-coating, requiring a large, flat substrate. Furthermore, the resulting structures are not perfectly symmetric and suffer from irregular edges [12].

Novel, sophisticated fabrication methods such as variable thickness DBs [13], superconducting Nb/Al bilayers [14] and normal-conducting heat-sinks [9] could further increase the sensitivity, but also add to the complexity of the fabrication process. The currently smallest, most sensitive nanoSQUIDs are based on a complicated process of directional evaporation of a superconducting material onto a pulled quartz tube. Vasyukov *et al.* fabricated a circular SQUID with a diameter of 50 nm, resulting in an inductance of 5.8 pH and a spin sensitivity below $1 \mu_B/\sqrt{\text{Hz}}$ making it capable of the detection of the spin of a single electron [15].

A different approach to creating superconducting devices using direct-write techniques is to start from a superconducting thin film and perform a FIB irradiation process to locally modify the electronic properties. This approach has allowed, for example, for the creation of high quality Josephson superconducting tunnelling junctions by irradiation with a focused He^+ ion beam [16]. NanoSQUIDs with a DB-width of 30 nm and a loop size of $1 \mu\text{m}$ were fabricated by Ga^+ FIB milling of a previously patterned Nb film in 1980 for the first time [5]. Recently, M. Wyss *et al.* used this technique to fabricate a SQUID on the tip of a capped AFM cantilever with a field sensitivity of $9.5 \text{ nT}/\sqrt{\text{Hz}}$ [17]. However, the Nb in the DBs deteriorates due to the implantation of Ga and amorphization that occurs in the surface and up to 30 nm below it.

An alternative to resist-based techniques or directional evaporation are direct-write techniques, such as Focused Electron / Ion Induced Deposition (FEBID / FIBID), which constitute versatile techniques for the fabrication of nanostructures on substrates of arbitrary size and topography [18, 19]. These techniques do not require the use of a resist and the entire nanostructure can be fabricated in a single step. Typically performed in either dedicated FIB instruments or in FIB/Scanning Electron Microscope (SEM) equipments, which host columns of both ions and electrons, the procedure begins by introducing a gaseous precursor containing the element of interest into the process chamber, which then adsorbs on the substrate. Upon local irradiation of the adsorbed molecules with the focused beam, the precursor is decomposed into a non-volatile constituent, which permanently remains deposited on the surface, and into volatile by-products that are pumped away by the vacuum system of the instrument. The resulting deposit is patterned following the shape of the scan traced by the beam (fig. 1b). In the case of FIBID, concurrently with the deposition of the desired material, the FIB modifies the exposed material by ion implantation, amorphization and sputtering. In absence of a precursor gas these effects can be used to locally modify the physical properties of a given sample or to locally remove material by milling [20, 21].

The ability of FEBID/FIBID techniques to pattern very small features, together with their versatility for patterning on unconventional non-planar

surfaces, and the well-established superconducting properties of W-C or Nb-C based nanodeposits created either by FEBID [22] or FIBID [23], make these techniques very promising for the fabrication of nanoSQUIDs in a single writing step.

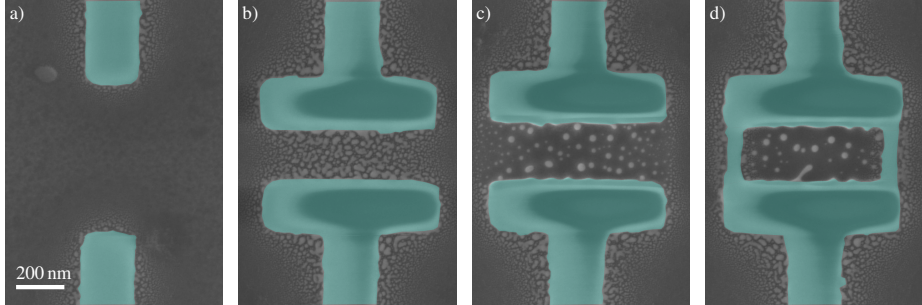


Figure 2: Artificially-colored SEM images of the fabrication procedure of a W-C-SQUID by FIBID. Blue represents the W-C material. a) First the leads connecting the SQUID to the Au leads are deposited. b) Secondly, two rectangular shapes are deposited. c) In the third step, the halo residing in the inner loop area is removed by a short step of FIB milling. d) In the last step, narrow (50 nm wide) nanowires forming the Dayem bridges are grown.

The superconducting properties of W-C fabricated by Ga^+ FIB irradiation of the commercially available precursor gas $\text{W}(\text{CO})_6$ are well studied. Planar Ga^+ FIBID W-C deposits exhibit a critical temperature of $T_c = (4 - 5) \text{ K}$ [24, 25, 26, 27], an upper critical magnetic field of $B_{c2} = (7 - 8.5) \text{ T}$ [28, 29, 30] and a critical current density of $J_c = (0.01 - 0.1) \text{ MA/cm}^2$ [25, 26, 27]. The London penetration depth is reported to be $\lambda_L = 850 \text{ nm}$ [31, 32] and the superconducting coherence length $\xi = (6 - 9) \text{ nm}$ [31, 32, 33, 26]. Nanostructures with linewidths down to 50 nm can be patterned with high precision and reproducibility [26].

Several remarkable applications for superconducting nanodevices fabricated by FIBID/FEBID have been reported thus far and are worth mentioning. W-C deposits have been used to induce proximity superconducting effects on other materials [34] and to study the spin polarization of magnetic materials in Andreev contacts [35]. Besides, narrow W-C nanowires fabricated by Ga^+ FIBID have been found to sustain long-range nonlocal flow of a single row of vortices, which could be of interest for manipulation of individual vortices in quantum technologies [36, 37], and allow tuning the value of the critical current by means of a gating voltage [32]. On the other hand, three-dimensional W-C nanostructures can be grown by Ga^+ FIBID as freestanding pick-up loops coupled to a SQUID [38] and can be designed to support unconventional vortex patterns [39]. Recently, K. Lahabi and co-workers have characterized the electronic and magnetic-field dependent properties of JJs created by FEBID [22]. Superconducting properties of planar and 3D superconducting NWs based on Nb-C nanodeposits and fabricated by FEBID and Ga^+ FIBID have also been studied [23, 40], with 3D nanowires exhibiting a higher critical temperature than their 2D counterparts.

The vast knowledge on the properties of W-C and on how to tune them as desired, together with its commercial availability, make the $\text{W}(\text{CO})_6$ precursor

the perfect candidate for a broad range of approaches for the fabrication of nanoSQUIDs. In a single-step process a combination of normal- and superconducting materials can be used to fabricate SQUIDs based on both SNS- and SsS-JJs.

In this work, we present a method to nanofabricate W-C based dc-SQUIDs with two DBs by means of focused Ga^+ ion beam induced deposition on flat Si/SiO_2 substrates. Section 2 describes the instruments and parameters used to carry out the experiments. Section 3.1 outlines the fabrication process that we have developed to fabricate nanoSQUIDs in a single writing step with high reproducibility and yield. In section 3.2 and section 3.3 the results of the characterization of the electric and magnetic properties of the dc-SQUIDs are outlined.

2 Experimental

The devices were grown on Si substrates covered with a thermally-grown, 300 nm thick SiO_2 surface layer. Prior to the deposition of the W-C nanoSQUIDs, a supporting Cr/Au structure, comprising the current and voltage leads for the electrical measurements of the devices, was patterned onto the substrates by optical lithography. A Süss MicroTec *MA6* mask aligner, equipped with a 405 nm mercury lamp, has been used to transfer the design to a $\sim 2.8 \mu\text{m}$ thick MMA resist layer. An electron beam deposition system (BOC EDWARDS *Auto 500*) has been used to metallize the sample with a 5 nm Cr and a 50 nm Au layer followed by lift-off in acetone. The fine contacting structure was carried out via EBL in a ThermoFisher Scientific *Helios NanoLab 600* FIB/SEM microscope controlled by a Raith *ELPHY Plus* pattern processor to a 270 nm layer of PMMA resist. The metallization and lift-off steps were then repeated as described above.

The nanofabrication and imaging of the W-C SQUIDs were performed in the same *Helios 600 NanoLab* FIB/SEM microscope, fitted with a Ga^+ ion column and a gas injection system (GIS) for precursor delivery. The imaging was performed with an electron beam current of 1.4 nA at an acceleration voltage of 5 kV. For the deposition of the W-C material, an ion beam current of 1.5 pA and an acceleration voltage of 30 kV were used. The volume per dose was $8.3 \times 10^{-2} \mu\text{m}^3/\text{nC}$, the overlap was set to 50 % and the dwell time was 500 μs . The base pressure of the FIB/SEM chamber was at 10^{-6} mbar, rising to 10^{-5} mbar during the injection of the $\text{W}(\text{CO})_6$ precursor gas. The nozzle of the GIS was positioned at a vertical distance of 50 μm and a in-plane displacement of 100 μm from the irradiation point.

The low temperature characterization of the magnetotransport properties of the sample was performed in a commercial Quantum Design *Physical Property Measurement System* instrument. The base temperature for the characterization was 2 K. The samples were connected to the instrument via ultrasonic wire-bonding of Al wires between the Cr/Au leads and the instrument sample holder.

3 Results and discussion

3.1 Device fabrication

The fabrication of the nanodevices has been performed in a series of sequential steps (fig. 2), which include the fabrication of both the Josephson junctions and the main body of the nanoSQUID. In order to obtain the highest possible lateral resolution when depositing the nanowires, the lowest ion beam current of the FIB (1.5 pA) was chosen. The current has been kept at this value for the whole structure.

After the process chamber was flushed with the precursor gas for 20 s, two 50 nm-thick W-C large leads were deposited to carry the injected current from the Au leads to the device (fig. 2a), taking 120 s. Thereafter, two 800 nm \times 200 nm rectangular pads with a thickness of 50 nm were deposited in contact with the leads fabricated in the previous step, and positioned 300 nm apart from each other (fig. 2b), taking 60 s.

During the deposition of materials by FIBID, a common problem is the undesired deposition of material in the vicinity of the irradiated area, an issue commonly referred to as *halo*. In the case of conductive deposits, the halo can carry part of the injected current. This is the reason why the halo deposit must be eliminated to ensure proper device functionality. We observed a significant amount of halo in between the pads, *i.e.* at the effective loop area of the SQUID. Thus the fabrication was paused until the precursor gas was completely evacuated from the chamber, taking 30 s, and a short FIB milling step of 2 s of the effective loop area was performed (fig. 2c) in order to remove the unwanted metallic deposits inside the inner loop area of the SQUID. Upon gas injection for 20 s, two nanowires acting as DBs were deposited connecting the two pads by their outer edges (fig. 2d), taking 5 s. In total, the full fabrication process of the SQUID takes less than 3 min plus the time required to deposit the leads which strongly depends on their length. The nanowires have a cross-sectional area of 50 nm \times 50 nm. The overall nominal loop area of the SQUID is 300 nm \times 700 nm.

3.2 Superconducting properties

In this section we present the superconducting properties of two identically grown SQUIDs, labelled A and B, in absence of an external magnetic field. The samples were cooled down to the base temperature of 2 K while constantly injecting a bias current $I_b = 0.2 \mu\text{A}$ and measuring the resistance, R . The temperature dependence of the resistance is shown in fig. 3a. Both SQUIDs exhibit a transition to the superconducting regime at $T_{c,A} = 4.29 \text{ K}$ and $T_{c,B} = 4.17 \text{ K}$, respectively. This is in good agreement with the results found in literature [33].

Thereafter, the current vs. voltage dependence was measured to obtain the critical current, shown in fig. 3b. One can notice several transitions, attributed to, both the contact pads and the DBs. A quantitative analysis indicates that the critical current of the DBs equals $I_{c,A} = 8.51 \mu\text{A}$ and $I_{c,B} = 7.98 \mu\text{A}$ for sample A and B, respectively. Although DB-SQUIDs are expected to exhibit hysteretic behavior due to dissipation of heat in the normal conducting state of the constrictions [1] we do not observe a hysteresis in the I-V characteristics. We attribute the suppression of the hysteresis and the high transition width to an increase of the effective temperature in the noise parameter $\Gamma = k_B T_{\text{eff}}/E_J$ due

to noise in the bias current [2]. The normal state resistance of the full structure, *i.e.* above all transitions, is $R_{N,A} = 496 \Omega$ and $R_{N,B} = 493 \Omega$ for each sample. Both the critical current and the critical temperature are very similar for the two nanoSQUIDs, confirming the reproducibility of the fabrication procedure. However, the transition width of sample B is smaller than that of sample A.

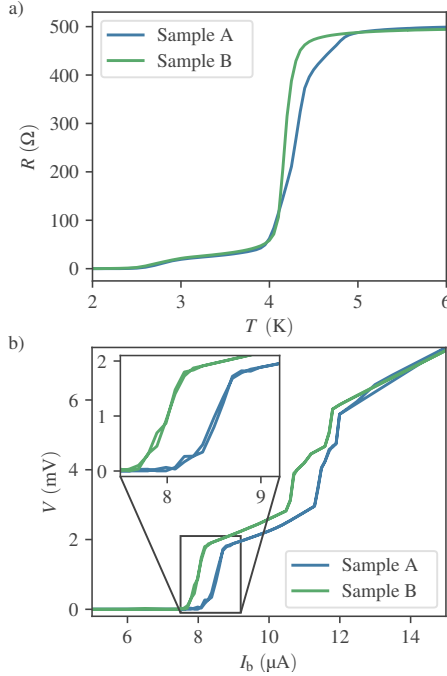


Figure 3: a) Temperature dependence of the resistance in the region of the transition from the normal to the superconducting state. b) I-V characteristics of the two samples. The different transitions are attributed to regions of different cross-sectional area.

3.3 Magnetic response

In a JJ the macroscopic wavefunctions of the two separated superconductors overlap resulting in a phase-dependent Josephson current flowing through, given by

$$I_J = I_0 \sin \delta(t) \quad (1)$$

where I_0 denotes the maximal Josephson current and δ the phase difference between the two superconductors. In a dc-SQUID the flux quantization requires the phase of the two JJs to fulfill the condition

$$\delta_1 + \delta_2 + 2\pi n = \frac{2\pi}{\Phi_0} \Phi_T \quad (2)$$

where the total flux is $\Phi_T = \Phi + LJ$, L being the inductance of the SQUID. The loop current J ensures this condition by raising or lowering the total flux by

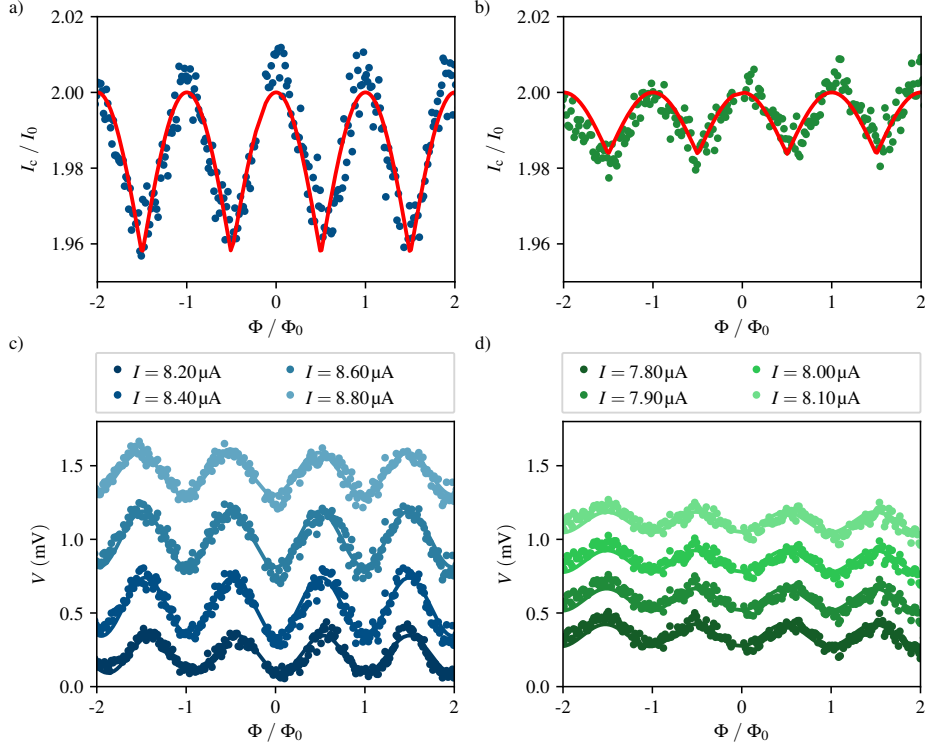


Figure 4: Electrical response of the devices to an external magnetic field at 2 K. a, b) Critical current in dependence of the magnetic flux threading the SQUID loop for sample A (a) and B (b). I_c is normalized by the maximal Josephson current of a single junction. The red curve denotes the fit of the data to the model $I_c = 2I_0|\cos(\Phi/\Phi_0)|$. c, d) Voltage at various bias currents $I \sim I_c$ in dependence of the magnetic flux threading the SQUID loop for sample A (c) and B (d). In all plots the magnetic flux is normalized by the magnetic flux quantum Φ_0 .

LJ . Assuming a negligible contribution of LJ and $I_{0,1} = I_{0,2} = I_0$ we obtain the dependence of the critical current of the nanostructure on the external flux as

$$I_c = 2I_0 \left| \cos \left(\frac{\pi\Phi}{\Phi_0} \right) \right|. \quad (3)$$

The quality of a SQUID can be characterized by the screening parameter

$$\beta_L = \frac{2LI_0}{\Phi_0}. \quad (4)$$

Equation (3) holds for $\beta_L \ll 1$ with a critical current modulation $\Delta I_c/2I_0 = 1$. For a non-negligible influence of LJ the critical current modulation decreases monotonically with an increasing screening parameter $\Delta I_c/2I_0 \approx 1/\beta_L$. This property allows one to estimate the inductance L of the SQUID.

To extract I_c we have measured several I-V characteristics of the SQUIDs at different values of perpendicularly-applied magnetic field. As the magnetic

flux threading the SQUID loop is quantized in integer multiples of the magnetic flux quantum Φ_0 , it is possible to attribute each period ΔH of the oscillation in $I_c(H)$ to a flux difference of $\Delta\Phi \equiv \Phi_0$. Figures 4a and 4b respectively show the dependence of the critical current of samples A and B (normalized to I_0) on the magnetic flux in units of Φ_0 . The red curve corresponds to the fit of the data to eq. (3) augmented by an offset current I_{off} in order to account for the non-negligible β_L :

$$\frac{I_c}{I_0} = \left| \cos \left(\frac{\pi\Phi}{\Phi_0} \right) \right| + I_{\text{off}}. \quad (5)$$

The period of the oscillation in I_c is similar in the two samples, with $\Delta H_A = 64.0 \text{ Oe}$ and $\Delta H_B = 56.7 \text{ Oe}$. The effective areas $A_{\text{eff}} = \Phi_0/\mu_0\Delta H$ deducted from this result are $A_{\text{eff},A} = 0.323 \mu \text{m}^2$ and $A_{\text{eff},B} = 0.365 \mu \text{m}^2$. These are greater than the geometric loop area of $A_{\text{geom}} \approx 0.175 \mu \text{m}^2$ which is to be expected due to the contribution of the kinetic inductance to the total inductance of the SQUID. Due to the high London penetration depth of W-C and the low thickness of the SQUIDs, the screening of the magnetic field is comparably low, yielding a high kinetic inductance [1].

The amplitude of the oscillations yields the dimensionless screening parameter $\beta_{L,A} = 47$ and $\beta_{L,B} = 122$, and the inductance of the devices, $L_A = 11 \text{ nH}$ and $L_B = 32 \text{ nH}$. The magnetic properties of the two SQUIDs are comparable to one another. However, the determination of I_c proved more error-prone due to the steeper transition in the I-V characteristics accounting for the minor differences between the samples.

Commonly, nanoSQUIDs are designed to have a screening parameter $\beta_L \approx 1$ and are furthermore optimized to have a low inductance L , which reduces the magnetic flux noise and thus improves the sensitivity to magnetic flux variations [1]. In DB-based SQUIDs based on Nb superconducting films ($\lambda_L = 47 \text{ nm}$ [41]) inductance values in the pH regime are typically achieved [1].

The common operation mode of a dc-SQUID is its use as a flux-to-voltage transducer, where a constant bias current $I_b \sim I_c$ is injected and the voltage V is measured, exhibiting a sinusoidal dependence on Φ . In the vicinity of $\Phi = (1/4 \pm n/2)\Phi_0$ a linear dependence of V on Φ is obtained. The strongest variation of V for a change of Φ is characterized by the transfer coefficient

$$V_\Phi|_{I_b} = \max \left(\frac{\partial V}{\partial \Phi} \right)_{I_b} \quad (6)$$

Thus, curves of constant I_b have been extracted from the I-V characteristics. Figures 4c and 4d show $V(\Phi)$ curves for various values of $I_b \sim I_c$ of sample A and B, respectively. In sample A the transfer coefficient is $V_\Phi = 1301 \mu \text{V}/\Phi_0$ for a bias current of $I_b = 8.5 \mu \text{A}$. In sample B we obtain $V_\Phi = 473 \mu \text{V}/\Phi_0$ at $I_b = 7.9 \mu \text{A}$. Typical values of the transfer function are in the range of $(10 - 100) \mu \text{V}/\Phi_0$ [1]. The high transfer coefficient is attributed to the high normal state resistance of the W-C nanoSQUIDs around 500Ω , due to the high resistivity of this material [33] in comparison to other structures reported in the literature, which is commonly around $(10 - 50) \Omega$ [42, 43].

4 Outlook

This fabrication procedure serves as a proof of concept for the fabrication of W-C nanoSQUIDs by means of Ga^+ FIBID. It has the prospect to be modified and augmented in various ways. The conduction regime (normal- or superconducting) of the W-C deposit can be controlled by deposition at various substrate temperatures (Cryo-FIBID) [44] or the use of an electron beam (FEBID) at different beam currents [22]. Thus the DBs can be readily replaced by a non-superconducting, FIBID-grown metal, resulting in SNS junctions. Thereby the fabrication of planar instead of sandwich-type SNS-JJ based nanoSQUIDs could be realized. A metallic heat-sink or a shunt resistor can be also added to the SQUID in a similar manner.

In recent years the development of SQUID on Tip (SOT) probes resulted in a new generation of Scanning SQUID Microscopes (SSMs) with unprecedented resolution and sensitivity for the mapping of the magnetic structure of a given surface [45, 46]. In this approach a SQUID is positioned on the tip of a pulled quartz tube via a three-step evaporation process. Lithographic methods require large, flat substrates and reach their limit with the high aspect ratio of the tip. The technique presented here poses a possible alternative approach for the fabrication of an SOT probe on commercially available Atomic Force Microscopy (AFM) cantilevers. The apex of the tip could be cut with the FIB and thereafter a SQUID could be deposited on the resulting flat area while maintaining the previously discussed flexibility in the SQUID design.

The comparably high inductance can be improved by both, a lower effective loop area and higher film thickness to enhance flux focusing. With Ga^+ FIBID the feasible linewidth is at around 50 nm and the London penetration depth is 850 nm. Recent studies showed that both parameters could be improved by the use of He^+ ions for the deposition of W-C nanowires. Nanowires with a linewidth down to 10 nm exhibit a London penetration depth of (400 – 812) nm [47, 48, 36] making the material a promising candidate for the improvement of the process developed in this article. Further work towards the optimization of the noise and sensitivity of the W-C SQUIDs is underway.

5 Conclusion

In this work we have successfully fabricated two W-C nanoSQUIDs with an inner loop area of $300 \text{ nm} \times 700 \text{ nm}$ in a fast Ga^+ FIBID-FIB process ($< 3 \text{ min}$). The SQUIDs exhibit a critical temperature of around 4.2 K and a critical current of around $8 \mu \text{A}$ at 2 K. Albeit the London penetration length of W-C is higher than that of similar devices of other materials, we have clearly observed oscillations of both the critical current and the voltage in dependence of the applied external magnetic field. The transfer coefficient is comparably high with up to $1301 \mu \text{V}/\Phi_0$, which we attribute to the high normal state resistance of the devices ($\sim 500 \Omega$).

The versatility of FIBID facilitates a high degree of freedom in the geometrical dimensions of the nanostructures and the substrate supporting the nanoSQUID, making the process a promising approach for the fabrication of SOT devices.

Author Contributions

F. S. performed the sample growth and the magnetotransport experiments, analyzed the data and wrote the first draft of the manuscript. P.O. contributed to the sample growth, data interpretation and the writing of the manuscript. S.S. and J.M.D.T. got the funding, supervised the research and contributed to the data interpretation and the writing of the manuscript.

Conflicts of interest

There are no conflicts to declare.

Acknowledgements

This research was supported by the European Commission under H2020 FET Open grant ‘FIBsuperProbes’ (number 892427), by the Spanish Ministry of Science through the grant PID2020-112914RB-I00, from CSIC through projects PIE202060E187 and Research Platform PTI-001, and by Gobierno de Aragón through the grant E13_20R with European Social Funds (Construyendo Europa desde Aragón). The following networking projects are acknowledged: Spanish Nanolito (RED2018-102627-T) and COST-FIT4NANO (action CA19140). Authors would like to acknowledge the use of Servicio General de Apoyo a la Investigación-SAI, Universidad de Zaragoza and the technical support provided by the LMA technicians at Universidad de Zaragoza. Furthermore we thank Julian Linek of the Physical Institute of the University of Tübingen (EKU) for the fruitful discussions.

References

- [1] Maria José Martínez-Pérez and Dieter Koelle. “NanoSQUIDS: Basics & recent advances”. In: *Physical Sciences Reviews* 2.8 (2017), p. 20175001. DOI: [doi:10.1515/psr-2017-5001](https://doi.org/10.1515/psr-2017-5001).
- [2] Alex I. Braginski and John Clarke. “The SQUID Handbook”. In: John Wiley & Sons, Ltd, 2004. Chap. 2, pp. 29–92. ISBN: 9783527603640. DOI: <https://doi.org/10.1002/3527603646.ch1>.
- [3] F. London. *Superfluids: Macroscopic theory of superconductivity*. Structure of matter series. Wiley, 1950.
- [4] B.D. Josephson. “Possible new effects in superconductive tunnelling”. In: *Physics Letters* 1.7 (1962), pp. 251–253. ISSN: 0031-9163. DOI: [https://doi.org/10.1016/0031-9163\(62\)91369-0](https://doi.org/10.1016/0031-9163(62)91369-0).
- [5] R. F. Voss et al. *Ultra low noise DC SQUIDS*. Germany: de Gruyter, 1980. ISBN: 3-11-008063-X.
- [6] M. B. Ketchen, T. Kopley, and H. Ling. “Miniature SQUID susceptometer”. In: *Applied Physics Letters* 44.10 (1984), pp. 1008–1010. DOI: [10.1063/1.94601](https://doi.org/10.1063/1.94601).

- [7] W. Wernsdorfer et al. “DC-SQUID magnetization measurements of single magnetic particles”. In: *Journal of Magnetism and Magnetic Materials* 145.1 (Mar. 1995), pp. 33–39. ISSN: 0304-8853.
- [8] John Gallop et al. “Miniatute dc SQUID devices for the detection of single atomic spin-flips”. In: *Physica C: Superconductivity* 368.1 (Mar. 2002), pp. 109–113. ISSN: 0921-4534.
- [9] S. K. H. Lam and D. L. Tilbrook. “Development of a niobium nanosuperconducting quantum interference device for the detection of small spin populations”. In: *Applied Physics Letters* 82.7 (2003), pp. 1078–1080. DOI: 10.1063/1.1554770.
- [10] P. W. Anderson and A. H. Dayem. “Radio-Frequency Effects in Superconducting Thin Film Bridges”. In: *Phys. Rev. Lett.* 13 (6 Aug. 1964), pp. 195–197. DOI: 10.1103/PhysRevLett.13.195.
- [11] W Wernsdorfer. “From micro- to nano-SQUIDs: applications to nanomagnetism”. In: *Superconductor Science and Technology* 22.6 (May 2009), p. 064013. DOI: 10.1088/0953-2048/22/6/064013.
- [12] C P Foley and H Hilgenkamp. “Why NanoSQUIDs are important: an introduction to the focus issue”. In: *Superconductor Science and Technology* 22.6 (May 2009), p. 064001. DOI: 10.1088/0953-2048/22/6/064001.
- [13] V. Bouchiat et al. “Josephson junctions and superconducting quantum interference devices made by local oxidation of niobium ultrathin films”. In: *Applied Physics Letters* 79.1 (2001), pp. 123–125. DOI: 10.1063/1.1382626.
- [14] D. Hazra, J. R. Kirtley, and K. Hasselbach. “Nano-superconducting quantum interference devices with suspended junctions”. In: *Applied Physics Letters* 104.15 (2014), p. 152603. DOI: 10.1063/1.4871317.
- [15] Denis Vasyukov et al. “A scanning superconducting quantum interference device with single electron spin sensitivity”. In: *Nature Nanotechnology* 8.9 (Sept. 2013), pp. 639–644. ISSN: 1748-3395. DOI: 10.1038/nnano.2013.169.
- [16] Shane A. Cybart et al. “Nano Josephson superconducting tunnel junctions in $\text{YBa}_2\text{Cu}_3\text{O}_7-\delta$ directly patterned with a focused helium ion beam”. In: *Nature Nanotechnology* 10.7 (July 2015), pp. 598–602. ISSN: 1748-3395. DOI: 10.1038/nnano.2015.76.
- [17] M. Wyss et al. 2021. arXiv: 2109.06774 [cond-mat.mes-hall].
- [18] Ivo Utke, Patrik Hoffmann, and John Melngailis. “Gas-assisted focused electron beam and ion beam processing and fabrication”. In: *Journal of Vacuum Science & Technology B: Microelectronics and Nanometer Structures Processing, Measurement, and Phenomena* 26.4 (2008), pp. 1197–1276. DOI: 10.1116/1.2955728.
- [19] Pablo Orús, Rosa Córdoba, and José María De Teresa. “Focused ion beam induced processing”. In: *Nanofabrication*. 2053-2563. IOP Publishing, 2020. Chap. 5, pp. 1–28. ISBN: 978-0-7503-2608-7. DOI: 10.1088/978-0-7503-2608-7ch5.

[20] L.A. Giannuzzi and F.A. Stevie. “A review of focused ion beam milling techniques for TEM specimen preparation”. In: *Micron* 30.3 (1999), pp. 197–204. ISSN: 0968-4328. DOI: [https://doi.org/10.1016/S0968-4328\(99\)00005-0](https://doi.org/10.1016/S0968-4328(99)00005-0).

[21] D. Petit et al. “Nanometer scale patterning using focused ion beam milling”. In: *Review of Scientific Instruments* 76.2 (2005), p. 026105. DOI: 10.1063/1.1844431.

[22] Tycho J. Blom et al. “Direct-Write Printing of Josephson Junctions in a Scanning Electron Microscope”. In: *ACS Nano* 15.1 (Jan. 2021), pp. 322–329. ISSN: 1936-0851. DOI: 10.1021/acsnano.0c03656.

[23] Fabrizio Porrati et al. “Crystalline Niobium Carbide Superconducting Nanowires Prepared by Focused Ion Beam Direct Writing”. In: *ACS Nano* 13.6 (June 2019), pp. 6287–6296. ISSN: 1936-0851. DOI: 10.1021/acsnano.9b00059.

[24] E.S. Sadki, S. Ooi, and K. Hirata. “Focused ion beam induced deposition of superconducting thin films”. In: *Physica C: Superconductivity and its Applications* 426-431 (2005), pp. 1547–1551. ISSN: 0921-4534. DOI: <https://doi.org/10.1016/j.physc.2005.02.151>.

[25] I. J. Luxmoore et al. “Low temperature electrical characterisation of tungsten nano-wires fabricated by electron and ion beam induced chemical vapour deposition”. In: *Thin Solid Films* 515.17 (June 2007), pp. 6791–6797. ISSN: 0040-6090. DOI: 10.1016/j.tsf.2007.02.029.

[26] R. Córdoba et al. “Magnetic field-induced dissipation-free state in superconducting nanostructures”. In: *Nature Communications* 4.1 (Feb. 2013), p. 1437. ISSN: 2041-1723. DOI: 10.1038/ncomms2437.

[27] D Spoddig et al. “Transport properties and growth parameters of PdC and WC nanowires prepared in a dual-beam microscope”. In: *Nanotechnology* 18.49 (Nov. 2007), p. 495202. DOI: 10.1088/0957-4484/18/49/495202.

[28] A. Helzel et al. “Nonlocal vortex motion in mesoscopic amorphous $Nb_{0.7}Ge_{0.3}$ structures”. In: *Phys. Rev. B* 74 (Dec. 2006), p. 220510. DOI: 10.1103/PhysRevB.74.220510.

[29] Jun Dai et al. “Superconductivity in Tungsten-Carbide Nanowires Deposited from the Mixtures of $W(CO)_6$ and $C_{14}H_{10}$ ”. In: *Japanese Journal of Applied Physics* 52.7R (July 2013), p. 075001. DOI: 10.7567/jjap.52.075001.

[30] Yi Sun et al. “Voltage-current properties of superconducting amorphous tungsten nanostrips”. In: *Scientific Reports* 3.1 (July 2013), p. 2307. ISSN: 2045-2322. DOI: 10.1038/srep02307.

[31] I. Guillamón et al. “Direct observation of melting in a two-dimensional superconducting vortex lattice”. In: *Nature Physics* 5.9 (Sept. 2009), pp. 651–655. ISSN: 1745-2481. DOI: 10.1038/nphys1368.

[32] Pablo Orús et al. “Critical current modulation induced by an electric field in superconducting tungsten-carbon nanowires”. In: *Scientific Reports* 11.1 (Sept. 2021), p. 17698. ISSN: 2045-2322. DOI: 10.1038/s41598-021-97075-z.

[33] E. S. Sadki, S. Ooi, and K. Hirata. “Focused-ion-beam-induced deposition of superconducting nanowires”. In: *Applied Physics Letters* 85.25 (2004), pp. 6206–6208. DOI: 10.1063/1.1842367.

[34] Jian Wang et al. “Proximity-Induced Superconductivity in Nanowires: Minigap State and Differential Magnetoresistance Oscillations”. In: *Phys. Rev. Lett.* 102 (24 June 2009), p. 247003. DOI: 10.1103/PhysRevLett.102.247003.

[35] S. Sangiao et al. “Ferromagnet–superconductor nanocontacts grown by focused electron/ion beam techniques for current-in-plane Andreev Reflection measurements”. In: *Solid State Communications* 151.1 (2011), pp. 37–41. ISSN: 0038-1098. DOI: <https://doi.org/10.1016/j.ssc.2010.10.028>.

[36] Rosa Córdoba et al. “Long-range vortex transfer in superconducting nanowires”. In: *Scientific Reports* 9.1 (Aug. 2019), p. 12386. ISSN: 2045-2322. DOI: 10.1038/s41598-019-48887-7.

[37] T. Golod, A. Iovan, and V. M. Krasnov. “Single Abrikosov vortices as quantized information bits”. In: *Nature Communications* 6.1 (Oct. 2015), p. 8628. ISSN: 2041-1723. DOI: 10.1038/ncomms9628.

[38] E. J. Romans et al. “Three-dimensional nanoscale superconducting quantum interference device pickup loops”. In: *Applied Physics Letters* 97.22 (Nov. 2010), p. 222506. ISSN: 0003-6951. DOI: 10.1063/1.3521262.

[39] Rosa Córdoba et al. “Three-Dimensional Superconducting Nanohelices Grown by He+-Focused-Ion-Beam Direct Writing”. In: *Nano Letters* 19.12 (Dec. 2019), pp. 8597–8604. ISSN: 1530-6984. DOI: 10.1021/acs.nanolett.9b03153.

[40] O. V. Dobrovolskiy et al. “Ultra-fast vortex motion in a direct-write Nb-C superconductor”. In: *Nature Communications* 11.1 (July 2020), p. 3291. ISSN: 2041-1723. DOI: 10.1038/s41467-020-16987-y.

[41] B. W. Maxfield and W. L. McLean. “Superconducting Penetration Depth of Niobium”. In: *Phys. Rev.* 139 (5A Aug. 1965), A1515–A1522. DOI: 10.1103/PhysRev.139.A1515.

[42] Roberto Russo et al. “Performances of niobium planar nanointerferometers as a function of the temperature: a comparative study”. In: *Superconductor Science and Technology* 27.4 (Mar. 2014), p. 044028. DOI: 10.1088/0953-2048/27/4/044028.

[43] Aico G. P. Troeman et al. “NanoSQUIDs Based on Niobium Constrictions”. In: *Nano Letters* 7.7 (July 2007), pp. 2152–2156. ISSN: 1530-6984. DOI: 10.1021/nl070870f.

[44] Rosa Córdoba et al. “Ultra-fast direct growth of metallic micro- and nano-structures by focused ion beam irradiation”. In: *Scientific Reports* 9.1 (Oct. 2019), p. 14076. ISSN: 2045-2322. DOI: 10.1038/s41598-019-50411-w.

[45] Amit Finkler et al. “Self-Aligned Nanoscale SQUID on a Tip”. In: *Nano Letters* 10.3 (Mar. 2010), pp. 1046–1049. ISSN: 1530-6984. DOI: 10.1021/nl100009r.

[46] Y. Anahory et al. “SQUID-on-tip with single-electron spin sensitivity for high-field and ultra-low temperature nanomagnetic imaging”. In: *Nanoscale* 12 (5 2020), pp. 3174–3182. DOI: 10.1039/C9NR08578E.

- [47] J. Basset et al. “High kinetic inductance microwave resonators made by He-Beam assisted deposition of tungsten nanowires”. In: *Applied Physics Letters* 114.10 (Mar. 2019), p. 102601. ISSN: 0003-6951. DOI: 10.1063/1.5080925.
- [48] Pablo Orús et al. “Superconducting properties of in-plane W-C nanowires grown by He+ focused ion beam induced deposition”. In: *Nanotechnology* 32.8 (Dec. 2020), p. 085301. DOI: 10.1088/1361-6528/abc91c.